Wet Dispersion Mechanism of Fine Aggregates in Multiphase Flow with Solid Beads Under Simple Shear

Daisuke Nishiura and Hide Sakaguchi
Dept. of Mathematical Science and Advanced Technology, Japan Agency for Marine-Earth Science and Technology, Kanagawa 236-0001, Japan

Atsuko Shimosaka
Dept. of Chemical Engineering and Materials Science, Doshisha University, Kyoto 610-0321, Japan

DOI 10.1002/aic.14614
Published online September 16, 2014 in Wiley Online Library (wileyonlinelibrary.com)

Clarifying the disintegration mechanism of aggregates in multiphase fluid flow coupled with beads and particulates is important for the optimum design of a wet dispersion process using a stirred media mill. Thus, we develop a numerical method for simulating multiphase flow with beads and particulates using a discrete element method and computational fluid dynamics, and we use the four-way coupling simulation to study the fluid-bead-particulate-coupled phenomenon that occurs in a simple shear box. The results show that the dominant force causing aggregate disintegration is the fluid force, rather than the bead contact force, because aggregates rarely collide with beads, contact force of which is too small to disintegrate aggregates. Furthermore, aggregates with strong aggregation force are effectively disintegrated by the fluid flow with a dominant high pure-shear rate induced near the bead surfaces by the expansive force, rather than the compressive force. © 2014 American Institute of Chemical Engineers *AIChE J*, 60: 4076–4085, 2014
Keywords: stirred media mill, discrete element method, direct numerical simulation, shear stress, collision

Introduction

Although many new and advanced nanoparticle-based functional materials have been developed, the high surface energy of nanoparticles induces the formation of aggregates that hinders the achievement of the target performance of the material. Disintegration of nanoparticle aggregates is thus a key process and is typically realized with a wet dispersion process. Wet dispersion is normally carried out using a stirred media mill in which rapidly rotating disks agitate a bed of grinding media (beads) that disperse the added particulate suspension. Aggregates are disintegrated by the shear flow of the suspension and collision with the beads. To optimize the dispersion process, we require a thorough understanding of the dispersion force applied to the aggregates from the fluid flow and bead collisions in such a shear flow. Such information will facilitate precise control of the dispersion state of the particulate suspension.

Empirical optimization of the dispersion process[1–4] is typically conducted because microscopic measurements of the fluid flow and bead motion or evaluation of the effective dispersion force on the disintegration of aggregates from experimental observations alone is extremely difficult. Numerical simulations are a useful tool for obtaining detailed information about the forces dominating the dispersion process or the bead behavior and fluid flow. However, these simulations have been based on simplifications that either neglect a calculation of the fluid flow and focus primarily on the bead behavior using the discrete element method (DEM[5,6])[7,8] or, conversely, estimate the bead behavior from a calculation of the viscous energy dissipated by turbulent flow in the absence of beads.[9,10] Even though there have been some studies that have treated both the bead behavior and fluid flow, they relied on one-way coupling, which neglects the forces acting on the fluid from the particle.[11–13] Accordingly, the present authors have simulated both the bead behavior and turbulent flow in a stirred media mill by considering bead–fluid interactions. In our earlier study, the power of the fluid shear, bead collisions, and friction were calculated, and the high power domain that develops in the mill was visually represented and quantified by using the DEM coupled with a large eddy simulation (LES).[14,15] However, in past studies, the interspatial fluid flow of the bead layer and the motion of the aggregates were not solved as a whole. Therefore, the actual force acting on aggregates in the dispersion process has not been evaluated exactly and the disintegration mechanism remains unclear.

Calculating the interspatial flow of the bead layer requires the use of a numerical method with a heavy computational cost such as direct numerical simulation (DNS). In addition, a fast numerical method is required to calculate the aggregate motion because there are a significantly larger number of particulates than beads in a stirred media mill. The limitations of the computational costs demand that the computational system used to calculate the aggregate motion is simplified. For example, there have been fundamental

Additional Supporting Information may be found in the online version of this article.

Correspondence concerning this article should be addressed to D. Nishiura at nishiura@jamstec.go.jp.

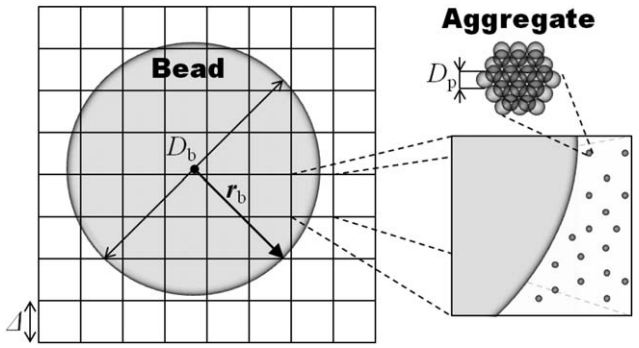

Figure 1. Computational geometry showing the particle location and grid used in the fluid calculation.

numerical studies of the aggregate disintegration process in simple shear flow,[16–19] but these studies did not consider the bead motion. We believe that the bead motion should be considered, even under simplified simple shear conditions, so that the influence of the complex shear flow induced by the bead motion can be investigated.

We have investigated the aggregate motion in the bead layer under simple shear flow to clarify the fundamental aggregate disintegration mechanism in a stirred media mill. The motion of the beads and particulates was calculated using the DEM, and the fluid flow around a bead was calculated exactly using a DNS model.[20] The particulate–fluid interactions were accounted for by using locally averaged Navier–Stokes equations and a two-phase flow model.[21,22] However, the excessive computational cost of these methods prevents a simulation of the aggregate disintegration process, and so to overcome this problem, we implemented a multigrid method[23] for the Poisson solver of the fluid flow that achieves near-optimal computational efficiency. For the particle motion, a highly efficient searching algorithm using a sort technique for pairs of particles in contact[24] was implemented in the DEM. The simulation program was completely parallelized on shared memory by using the OpenMP libraries.

Using this highly efficient simulation method, the fluid shear intensity was investigated, and the high-shear domain that develops around a bead was visually represented and quantified. The effect of bead collisions on the dispersion process was also investigated, and the probability of collisions between a bead and an aggregate was evaluated. In addition, the forces of the fluid shear and bead collision acting on the aggregates were investigated in detail, and an attempt was made to quantitatively evaluate the dominating force of the dispersion.

Numerical Method

The numerical method was developed to solve the multiphase flow in a box containing both the beads and particulates under simple shear conditions. To numerically evaluate the forces acting on the aggregates, we attempted to include a description of the interaction forces that was exact as possible. The bead and particulate motion was calculated using the DEM by taking into account the interactions between particles (e.g., bead to bead, bead to particulate, and particulate to particulate) and the interactions between the particles and the fluid. The interactions between the beads and the fluid were treated using the DNS model on a Cartesian grid (see Figure 1) that enables the turbulent flow around a bead to be reproduced if the grid size Δ is one-eighth of the bead size D_b.[20] We set D_b/Δ to 64 to exactly reproduce the particulate motion in the fluid flow around a bead. The interactions between the particulates and fluid, however, were treated using the locally averaged model[21] on the same Cartesian grid. In this study, it was not possible to use the DNS model to calculate the particulate–fluid interaction because of the huge computational cost owing to the sizes of the particulates, which are 1000 times smaller than a bead. However, we assumed that it was not necessary to calculate the particulate–fluid interaction at a high resolution using the DNS method because under the conditions considered here the particulate suspension is dilute and the Stokes number is very small ($\mathcal{O}(10^{-6})$). Thus, the particulate motion has a negligibly small effect on the fluid flow. Details of our numerical method are explained in the following subsections.

Fluid flow

The governing equations for the flow of a fluid containing beads and particulates are the continuity equation

$$\frac{\partial \varepsilon}{\partial t}+\frac{\partial \varepsilon u_j}{\partial x_j}=0 \tag{1a}$$

and the Navier–Stokes equation of motion

$$\frac{\partial \varepsilon u_i}{\partial t}+\frac{\partial \varepsilon u_i u_j}{\partial x_j}=\frac{\varepsilon}{\rho_f}\frac{\partial \tau_{ij}}{\partial x_j}+f_{bi}+f_{pi} \tag{1b}$$

based on the two-fluid model, where u denotes the fluid velocity and

$$\tau_{ij}=-pI_{ij}+\mu_f\left(\frac{\partial u_j}{\partial x_i}+\frac{\partial u_i}{\partial x_j}\right) \tag{2}$$

is the stress tensor, p is the static pressure, I is the unit tensor, ε is the fluid volume fraction, ρ_f is the fluid density, μ_f is the fluid viscosity, f_b is the bead–fluid interaction term, and f_p is the particulate–fluid interaction term. These equations are solved in a three-dimensional Cartesian geometry ($i,j\in\{1,2,3\}$) using the simplified marker and cell (SMAC) method. To solve for the fluid pressure efficiently, the multigrid Poisson solver[23] was implemented as a convergence acceleration method. In addition, the Poisson solver was parallelized using the Red-Black successive over relaxation (SOR) method.[25]

Particle motion

The governing equations for the individual particles are Newton's equations of motion

$$M\frac{\partial v_i}{\partial t}=T_i+F_i \tag{3a}$$

$$J\frac{\partial \omega_i}{\partial t}=R_i+W_i \tag{3b}$$

where v, ω, M, and J are the particle translational velocity, angular velocity, mass, and moment of inertia, respectively, and R and T are the torque and translational force, respectively, resulting from two-particle interactions such as bead–bead, bead–particulate, and particulate–particulate interactions. One interaction is a contact force represented by the Voigt model[26,27] that is generally used in the DEM, and another is the Derjaguin–Landau–Verwey–Overbeek (DLVO)

interaction,[28] which is an important force that determines the dispersion state of the particulates. Thus, in addition to the contact force, the van der Waals attraction force F_V and electrostatic repulsion force F_E according to DLVO theory were considered for the particulate motion as the particulate–particulate interaction

$$F_V = -\frac{AD_p}{24L^2} \tag{4}$$

$$F_E = 32\pi k_b T_\infty \rho_\infty D_p \tanh^2(e\psi/4k_b T_\infty) L_e e^{-L/L_e} \tag{5}$$

where the univalent ion concentration ρ_∞ and temperature T_∞ of the bulk solution were constants of 0.01 mol/L and 298 K, respectively. Here, A, k_b, e, ψ, L_e, and L are the Hamaker constant, Boltzmann constant, elementary charge, zeta potential, Debye length, and surface distance between particulates, respectively. Conversely, the DEM simulation is able to handle the viscoelastic force in multibody contact by using the Voigt model with a friction slider. In this model, the elastic spring force is based on the Hertz-Mindlin contact theory.[26,27] In addition, the viscous damping force is calculated using the damping coefficient analytically obtained by Tsuji et al.[29] The external forces F and W generated by the fluid flow are represented by different models depending on whether the particle is a bead or particulate. In consideration of these interaction forces, the motion of an individual particle was tracked by the numerical integration of Eqs. 3a and 3b using the leap-frog method. In addition, we implemented speed-up algorithms using a sort technique in the calculation of the pairwise interactions[24] because searching for interacting particle pairs and calculating the interaction force is computationally expensive.

Bead–fluid interaction model

To investigate the effect of the fluid flow around a bead on the aggregate disintegration, the bead–fluid interaction should be calculated to a high resolution using the surface integral of the fluid stress for momentum exchange at the bead–fluid interface rather than using an empirical model such as the locally averaged model used for the particulates. However, calculating the surface integral is computationally demanding, and so to improve the efficiency, we replace the surface integral of τ with a volume integral of the interacting force f_b.[20] The translational and rotational components of the interaction force acting on a bead are then

$$F_i = -\int_{V_b} f_{bi}\, dV \tag{6a}$$

$$W_i = -\int_{V_b} (\mathbf{r}_b \times \mathbf{f}_b)_i\, dV \tag{6b}$$

where the integral domain V_b is for all the grid elements including the bead, and the vector $\mathbf{r}_b$ is the relative position from the rotational center of the bead to the center of the corresponding grid element. We consider here the interacting force f_b as the force that modifies the velocity inside the computational grid element including the bead to be the volume-weighted average velocity

$$u_i = (1-\alpha)u_i' + \alpha U_i \tag{7}$$

where α is the volume fraction of the bead in a grid element, U is the velocity inside the bead, defined as

$$U_i = v_i + (\boldsymbol{\omega} \times \mathbf{r}_b)_i \tag{8}$$

and u' is the predicted velocity if the entire computational field was occupied by fluid. Thus, to satisfy the velocity field in Eq. 7, f_b is

$$f_{bi} = \alpha(U_i - u_i')/\Delta t \tag{9}$$

Particulate–fluid interaction model

On the basis of a locally averaged model, the particulate–fluid interaction force was obtained from the drag force correlation[21]

$$f_{pi} = \beta(\bar{v}_i - u_i)/\rho_f \tag{10}$$

which is applicable to a wide range of particulate concentrations. Here, $\bar{v}_i$ is the average velocity of the particulates within the computational grid element, and β is a drag coefficient that is dependent on the particle concentration. The drag coefficient is generally computed using an empirical model with the Ergun equation[30] for high concentrations and the Wen and Yu equation[31] for low concentrations. Note that the Ergun equation for the dense regime is necessary for calculating the particulate–fluid interaction, even though the particulate suspension is dilute in the entire system because the particulates can be locally consolidated when they are sandwiched between two beads or the aggregates become large. The fluid resistance force acting on the particulates is related to the opposing reactions of the interaction force f_p and fluid stress τ of Eq. 2 and can be expressed as

$$F_i = \frac{\pi D_p^3}{6}\left[\frac{\beta(u_i - v_i)}{1-\varepsilon} + \frac{\partial \tau_{ij}}{\partial x_i}\right] \tag{11}$$

The force should depend on the location of individual particulates in the computational grid element; however, the effect of fluid flow on the particulate motion is equal for all particulates within the same grid element because the physical quantities at the center of the grid element are used to calculate the fluid force for all particulates in the grid element. Therefore, to improve the accuracy of the fluid force calculation, the fluid velocity and stress at the location of an individual particulate were linearly interpolated between adjacent grid elements, and these interpolated quantities were used in Eq. 11.

Note that the fluid force acting on the rotational component of the particulate motion is ignored in this study because a model for the rotational force has not yet been constructed in the regime of a locally averaged model.

Computational procedure

An overview of the time-marching procedure for our numerical simulation is shown in Figure 2. The fluid field (velocity and pressure) is solved using the parallelized SMAC method with the multigrid SOR solver assuming that there are no beads in the field; Eq. 1b without f_b is solved to satisfy the continuity of Eq. 1a. The obtained velocity is then modified to satisfy the velocity given in Eq. 7 using the interaction force f_b of Eq. 9, and the time marching for the fluid calculation is completed. After this, the particle motion (velocity and position) is calculated using the parallelized DEM. The fluid force defined in Eqs. 6a and 6b for a bead or Eq. 11 for a particulate and the interparticle force are calculated, and the motion equation is numerically integrated using the leap-frog method. These steps are iterated in

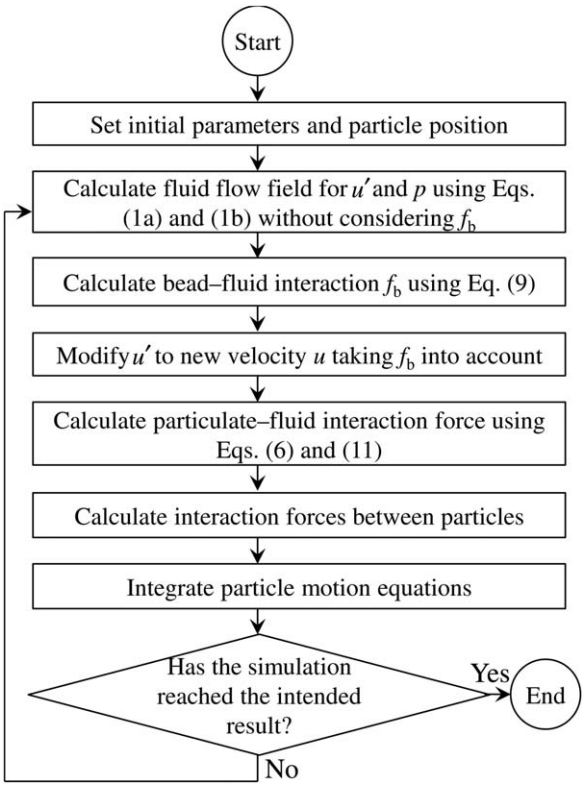

Figure 2. Flowchart of the numerical simulation.

constant discrete time units until the simulation reaches the intended result. Note that the discrete time step of the fluid calculation is set to a value that is 100 times larger than that of the particle calculation in the DEM because of the differences in the Courant–Friedrichs–Lewy condition of the fluid calculation method and DEM. Therefore, the particle calculation is iterated 100 times during one time iteration of the fluid calculation.

Simulation settings for the dispersion process in a simple shear box

Our numerical simulation is carried out in a simple shear box containing beads and particulates, as shown in Figure 3. Periodic boundary conditions are set in the horizontal (x- and y-axes) directions against the shear plane. For the boundary of the vertical (z-axis) direction, nonslip and nonpermeable boundary conditions are set for the fluid flow calculation, and a friction wall is set for the DEM calculation of the particle motion. A simple shear field is induced by lateral movement in the x-direction of the upper and lower wall boundaries, whose velocities are equal and opposite.

As a preprocessing step, only the beads are placed at regular locations and simulated inside the shear box. This creates a steady-state condition, and aggregates of a homogeneous size and shape are placed regularly into the voids of the bead layer in the shear box. A single aggregate is modeled as a spherical, hexagonal-close-packed assemblage of 57 particulates. The diameter of an aggregate is thus five times larger than that of a single particulate. The surface distance between neighboring particulates is set to 0.4 nm, and we set the DLVO force to be constant, even if the particulates are closer than 0.4 nm, so as to avoid an infinite van der Waals attractive force. In the practical wet dispersion process for nanoparticles using a stirred media mill, the effects of gravity and centrifugal force on the bead motion do not appear to be negligible, because the bead layer is densely packed in the gravitational and centrifugal directions. This means the gravity and centrifugal force can potentially influence the probability of bead–bead contact and the velocity of the interspatial flow in the bead layer. However, in this simulation, gravity and centrifugal force are not considered to conduct a simple investigation of the effects of bead motion and fluid flow on the disintegration of aggregates in the uniform simple shear system, in which deviations in particle concentration and interaction forces are rare.

The physical properties of the fluid and particles are listed in Table 1, and the simulation conditions are listed in Table 2. The physical properties of the bead and particulate are based on the measured values for ZrO_2 bead and $BaTiO_3$ particulate, respectively. However, the Young's modulus used for the simulation is less than that of real materials because of the limitation in discretizing the time integration in DEM. The Young's modulus significantly influences the amount of overlap between particles in contact but hardly influences the bead motion and the aggregate disintegration because the elastic spring force is correctly calculated. Moreover, for simplicity, the dissipation term of particulate–particulate contact due to viscous damping and friction is not considered, because the interaction force between particulates is dominated by the DLVO force, rather than the contact force. Therefore, the time step size in discretizing the time integration for particulate calculation in DEM depends on not only the Voigt model but also the DLVO model. We carefully choose the time step size in DEM to calculate the force in the potential curve of DLVO theory with sufficient time resolution. For the fluid, the density and viscosity are based on the measured values for $BaTiO_3$ suspensions of 30 vol %. Here, only the motions of some representative particulates in the 30 vol % suspension are calculated in the simulation; the motion of the entire dense suspension cannot be calculated because of the computational cost involved. The computational time for one execution (the

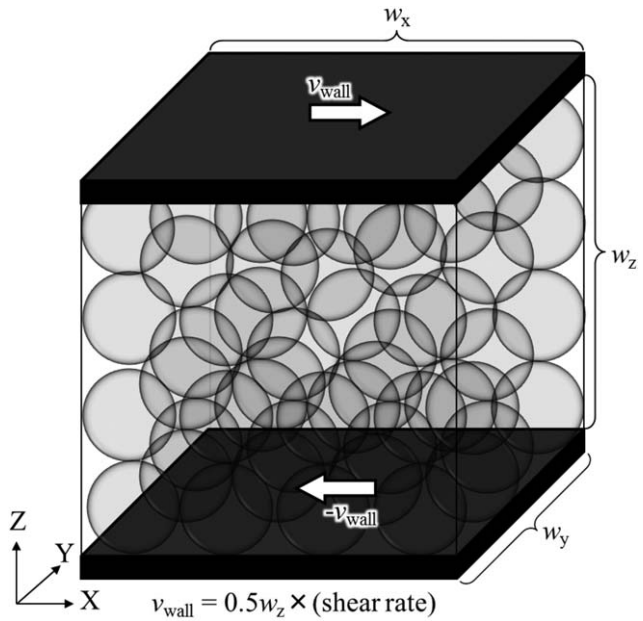

Figure 3. Overview of the simple shear box used in the numerical simulations.

Table 1. Material Properties

	Bead	Particulate	Wall	Fluid
Density [kg/m^3]	6000	6000	6000	1238
Viscosity [mPa s]	–	–	–	7.5
Diameter [μm]	100	0.1	–	–
Young's modulus [MPa]	21	0.01	21	–
Poisson's ratio [-]	0.32	0.2	0.32	–
	Bead–Bead (–Wall)	Particulate–Particulate		Particulate–Bead (–Wall)
Coefficient of restitution [-]	0.9	1.0		0.2
Coefficient of friction [-]	0.5	0.0		0.2
Zeta potential [mV]	–	32.2		–
Debye length [nm]	–	3.21		–

real physical time is 0.625 ms) was about 2 weeks when using two CPUs (Intel Xeon E7-4870).

Analysis of Wet Dispersion Process

In this section, we discuss the overall aspects of the bead-particulate-fluid-coupled phenomenon induced by simple shear and investigate the detailed disintegration process by varying the DLVO-interaction-dependent aggregation force. We clarify the extent to which the fluid flow and bead collisions are able to disintegrate aggregates, and the degrees of the fluid force and bead contact force acting on aggregates are investigated. The dominant force for aggregate disintegration in a simple shear system is determined, and the role of the beads in the wet dispersion process is also discussed.

Overall aspects of the simple shear system

To understand the overall phenomenon revealed in the simulated simple shear box, snapshots of the fluid flow at a shear rate of 4000 s^{-1} are shown in Figure 4 (also see Supporting Information Video 1). Figure 4b confirms that the pure-shear rate developed in the (*xy*-) plane parallel to the shear but that there was also some slight shearing in the vertical (*z*-) direction. The localization of the pure shear in the parallel and vertical directions is due to the translational and rotational motion of the beads, respectively, induced by the shear field. In particular, the rotational motion, with an average velocity of about 300 rad/s, enhances the large pure shear around the bead surface (Figure 4a). This trend is also quantitatively represented in Figure 5, which shows that the pure-shear rate is highly closer to the bead surface. Note that the pure-shear rate shown in Figure 5 should be a maximum at the bead surface, but this was not recreated in our simulations because we used a Cartesian grid of approximately 1.6 μm elements in the fluid calculation; rotational motion within the bead affects the pure-shear rate to a distance of approximately 1.6 μm from the surface of the bead.

Table 2. Simulation Conditions

Test Sample No.	Run 1	Run 2	Run 3	Run 4
Hamaker constant [10^{-20} J]	0.63	1.12	1.99	6.30
Shear rate [s^{-1}]	4000			
Shear box size ($w_x \times w_y \times w_z$) [mm]	$0.4 \times 0.346 \times 0.4$			
Number of grids in CFD [-]	$256 \times 256 \times 256$			
Number of beads [-]	64			
Number of particulates [-]	2,220,207			
Time step of DEM [ns]	0.05			
Time step of CFD [ns]	5.0			

A snapshot of the bead and particulate motion and details near three beads are shown in Figure 6 (also see Supporting Information Video 2). In Figure 6a (Supporting Information

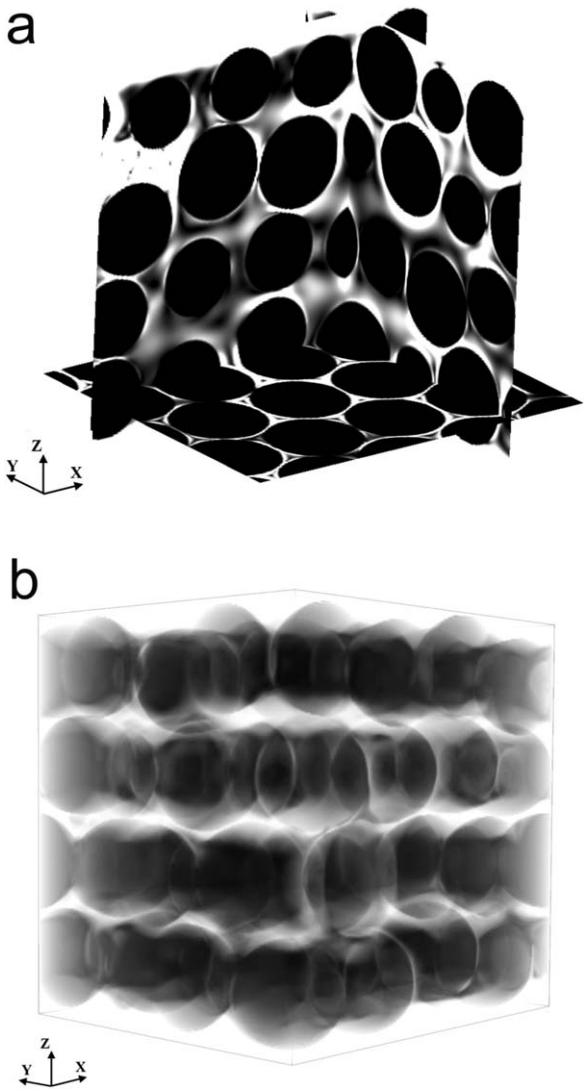

Figure 4. Spatial distribution of the rate of pure-shear strain in the simple shear box: (a) cross sections and (b) overall view where the change in the contour color from black to white represents an increasing strain rate from 1000 to 5000 s^{-1}.

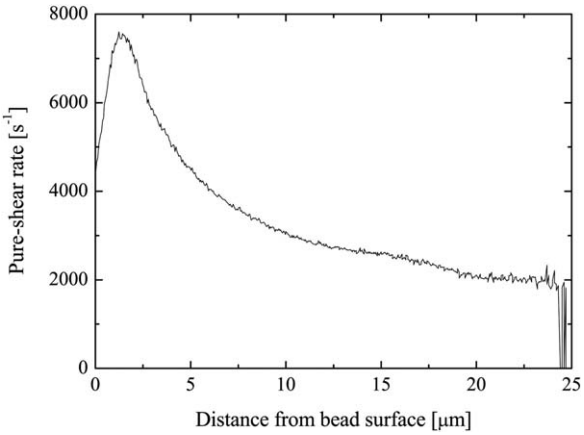

Figure 5. Relationship between the distance from the bead surface to a computational grid element and the pure-shear rate.

Video 2a), the large grey objects are beads and the small black objects are the particulates. We were able to confirm that the beads were shifted in the shear direction by the global fluid flow and that the local fluid flow induced by the bead motion complicates the particulate motion. In the detailed view in Figure 6b (Supporting Information Video 2b), aggregates, which are shown in gold, appear to have disintegrated around the local bead surface because of the effect of the fluid flow or bead collisions (note that in this figure and video, shadows of the objects are rendered to enhance the sense of distance between the bead and aggregate). The aggregates around the bead surface appear to be well disintegrated. However, the details of the aggregate disintegration mechanism cannot be clarified from these pictures and animations. Note that the aggregates around the upper and lower walls shown in Figure 6a have disintegrated to a larger extent; however, this is due to wall effects and is not of interest for this study. We thus limit the following investigation to internal regions of the box.

Influence of bead collisions and fluid shear flow

To investigate the influence of bead collisions and fluid shear flow on the aggregate disintegration, we defined the degree of disintegration S^t at time t as

$$S^t = \frac{s^t}{s^0}, \quad s^t = \sum_a d_a^t \tag{12}$$

where a labels a single particulate in the aggregate, and d_a is the distance between the center of particulate a and the center of the aggregate. If the value of S is larger than 1.1, then the aggregate is deemed to have disintegrated. This corresponds to the surface distance between the nearest-neighbor particulates in the aggregate being larger than 0.01 μm, which is one-tenth of the particulate diameter. Note that two particles separated by a surface distance of 0.01 μm have fully overcome the potential energy barrier of the DLVO interaction for all test conditions as shown in Figure 7.

The number ratio of disintegrated aggregates with $S > 1.1$ after a shearing time of 0.625 ms (i.e., a shear strain of 2.5) is shown in Table 3. The DLVO force between particulates aggregated at the primary minimum point (0.4 nm) of the potential energy curve is listed as the aggregation force. The simple shear system disintegrates fewer aggregates as the

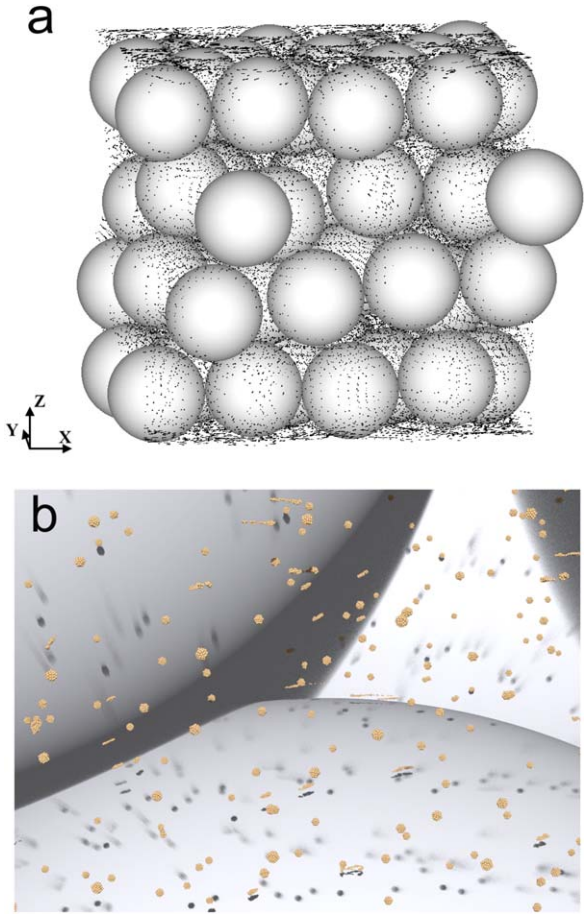

Figure 6. Bead and particulate motion induced by the simple shear field: (a) overall and (b) detailed views.

aggregation force increases in Runs 1 to 4, and no aggregate disintegration takes place in Run 4. For these disintegrated aggregates, we investigated the effect of bead collisions, and Table 4 shows the number ratio of disintegrated aggregates ($S > 1.1$) colliding with a bead at the time of the aggregate disintegration. Aggregates are rarely sandwiched between two beads, and even for the collision with one bead, the ratio is lower than 4% in all test cases. Note that it is possible

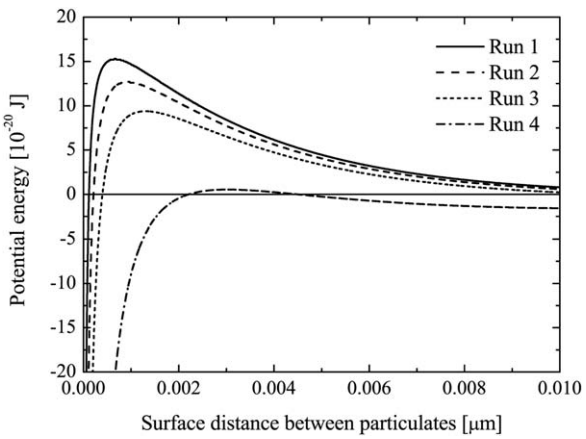

Figure 7. Potential energy curve of the DLVO interaction between particulates for each test sample.

Table 3. Number Ratio of Disintegrated Aggregates (Disintegration Ratio) and Aggregation Force for each Test Condition

Test Sample No.	Run 1	Run 2	Run 3	Run 4
Disintegration ratio [%]	76.6	19.4	2.4	0.0
Aggregation force [nN]	0.099	0.227	0.453	1.580

that this ratio is slightly overestimated because our simulation cannot take into account a lubrication force[32,33] between beads and aggregates because of the lack of spatial resolution in the fluid calculation. It seems that the effect of bead collisions on the aggregate disintegration is negligibly small; nevertheless, the number ratio of aggregates colliding with beads increases with increasing aggregation force. We could conclude from this result that aggregates with a strong aggregation force are disintegrated by the effect of bead collisions, but the effect of bead collisions on intact aggregates, shown in Table 5, reveals that the number ratio of aggregates that have collided with a bead during a simulation time of 0.625 ms also increases with increasing aggregation force. Therefore, we doubt that aggregates are effectively disintegrated by colliding with beads.

To clarify the effect of the fluid shear flow on the aggregate disintegration, the (relative frequency) density distributions of the pure-shear rates at the locations of the aggregates are shown in Figure 8. The relative frequency density is defined as the number ratio of the aggregates in a bin divided by the bin width. Note that we are interested in only the pure-shear flow that removes the rotational component from the simple shear flow because the rotational flow does not deform aggregates in shear flow. For the disintegrated aggregates in Figure 8a, the distribution shifts to larger pure-shear rates with increasing aggregation force (Run 1 to Run 3). This trend is also seen for the intact aggregates (Figure 8b), but the differences in the distributions of Runs 2, 3, and 4 are small. However, in comparison with the distributions for disintegrated aggregates, the distributions of the intact aggregates all peak at lower pure-shear rates. These results, therefore, suggest that aggregates are effectively disintegrated by the fluid flow shear stress because aggregates with a strong aggregation force are disintegrated in fluid flow with a high pure-shear rate.

Figure 9 shows the density distributions of the distance between an aggregate and the surface of the nearest bead. The distributions in the initial state of the simulation are shown for reference. We can confirm from Figure 9a that disintegrated aggregates are located at positions closer to the bead when the aggregation force increases. In contrast, the number of intact aggregates near a bead decreases in comparison with the number in the initial state (Figure 9b). These results are consistent with those in Figure 8 because

Table 4. Number Ratio of Disintegrated Aggregates (with $S>1.1$) Colliding with Beads at the Time of the Aggregate Disintegration

	Number Ratio of Aggregates [%]			
Test Sample No.	Run 1	Run 2	Run 3	Run 4
Sandwiched between two beads	0.04	0.18	0.00	N/A
In a collision with only one bead	0.52	1.05	3.78	N/A
Total	0.56	1.23	3.78	N/A

Table 5. Number Ratio of Intact Aggregates (with $S<1.1$ at $t=0.625$ ms) that have Collided with a Bead During the First 0.625 ms

	Number Ratio of Aggregates [%]			
Test Sample No.	Run 1	Run 2	Run 3	Run 4
Sandwiched between two beads	0.00	0.04	0.12	0.21
In a collision with only one bead	0.81	0.94	1.29	1.52
Total	0.81	0.98	1.41	1.73

the fluid shear flow develops around the bead surface as shown in Figure 5. As a result, strongly bonded aggregates are disintegrated by the strong shear flow induced in the near bead surface. In addition, the probability of a collision between a bead and an aggregate increases as the aggregation force increases because aggregates are closer to the beads. We believe that this results in an increase in the number ratio of aggregates that have collided with a bead, as shown in Tables 4 and 5.

Consequently, we can conclude that the effect of fluid shear flow on the aggregate disintegration is larger than that of bead collisions.

Effective force for aggregate disintegration

To determine the most effective force for aggregate disintegration, we investigated the forces acting on the aggregates

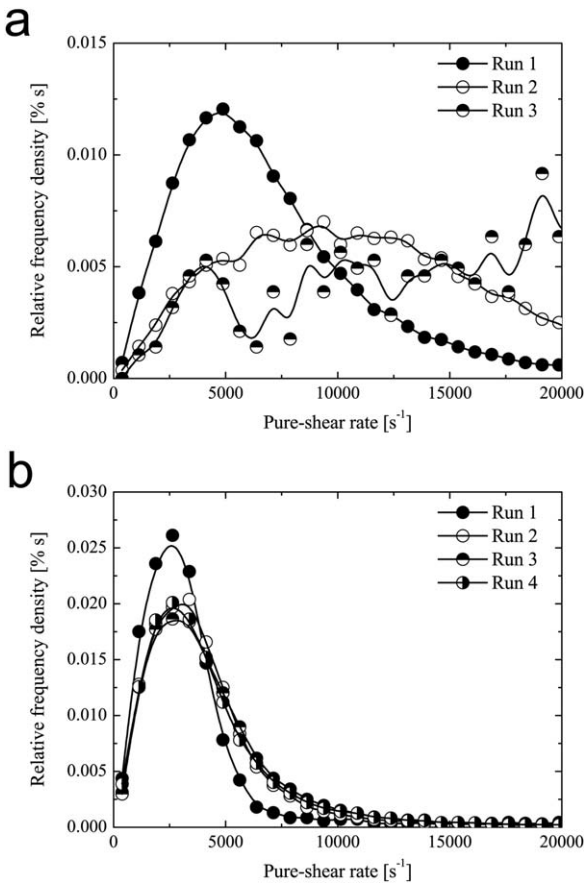

Figure 8. Density distribution of the pure-shear rate of the fluid flow at the aggregate locations: (a) disintegrated aggregates and (b) intact aggregates.

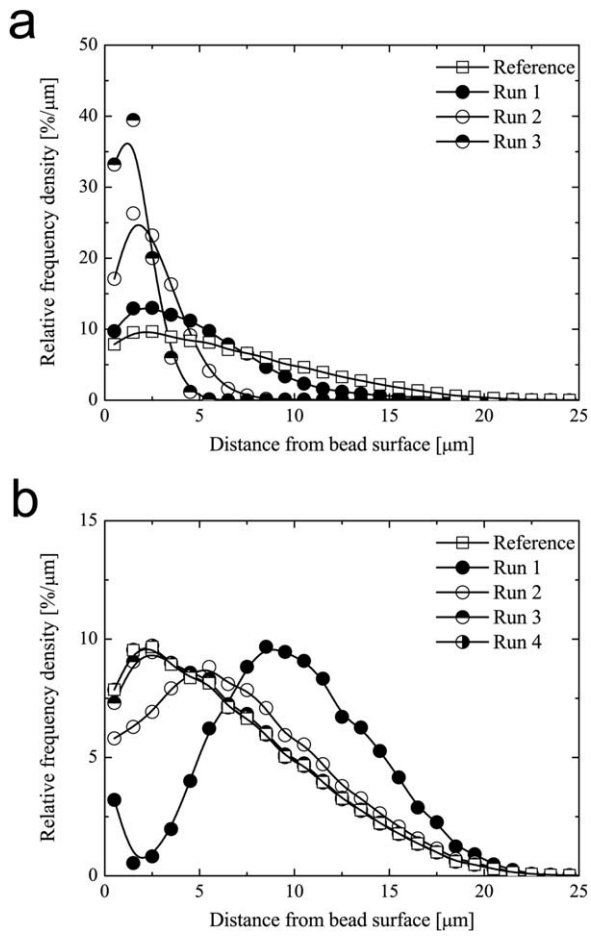

Figure 9. Density distribution of the distance between an aggregate and the nearest bead surface: (a) disintegrated aggregates and (b) intact aggregates.

due to bead collisions and fluid flow. The normal force F_N and tangential force F_T are calculated as

$$F_N = \sum_a \mathbf{f}_a \cdot \mathbf{n}_a \tag{13a}$$

$$F_T = \sum_a (\mathbf{f}_a - |\mathbf{f}_a \cdot \mathbf{n}_a| \mathbf{n}_a) \tag{13b}$$

where $\mathbf{n}_a$ is the normalized unit vector from the center of an aggregate to the position of particulate a, and $\mathbf{f}_a$ is the force vector acting on particulate a. For example, $\mathbf{f}_a$ is defined as F_i in Eq. 11 for the fluid force and as T_i in Eq. 3a for the contact force between a particulate and bead. The contact force distributions are shown in Figure 10. Because there is not enough data for statistics to be calculated for the other conditions, that is, the low numbers of aggregates that had collided with a bead (see Tables 4 and 5), only the data from Run 1 are shown. However, the contact force distribution will be almost the same in all test cases because it does not depend on the aggregation force. From Figure 10, we can see that the distributions of the disintegrated and intact aggregates are similar for both the tangential and normal components. However, if the contact force is effective in disintegrating aggregates, then we would expect that the force distribution for disintegrated aggregates is shifted to higher force values with respect to that for intact aggregates. In contrast, for the fluid force (Figure 11), the force distribution for the disintegrated aggregates is remarkably different from that for the intact aggregates. Note that because the distribution for intact aggregates was almost the same in all test cases, only the data of Run 1 are shown in the figure. In addition, the distribution of the tangential force shifts to larger forces with increasing aggregation force. Therefore, strongly bonded aggregates are disintegrated by a stronger tangential force of the fluid flow. The most interesting thing is that the distribution of the normal force in Figure 11b shifts from a negative (compression) region to a positive (expansion) region with increasing aggregation force. This means that the expansive force is more dominant than the compressive force in affecting the disintegration of aggregates with a strong aggregation force. From these results, we expect that the aggregate disintegration mechanism in the wet dispersion process using media beads can be understood as follows:

1. Aggregates are essentially disintegrated by the fluid force due to the strong shear flow around bead surfaces.

2. For the disintegration of weakly bonded aggregates, the compressive fluid force is dominant when the aggregates are close to beads or when aggregates enter the narrow channels between beads.

3. For the disintegration of strongly bonded aggregates, the expansive fluid force is dominant when the aggregates are away from the beads or when the aggregates leave the narrow channels between beads.

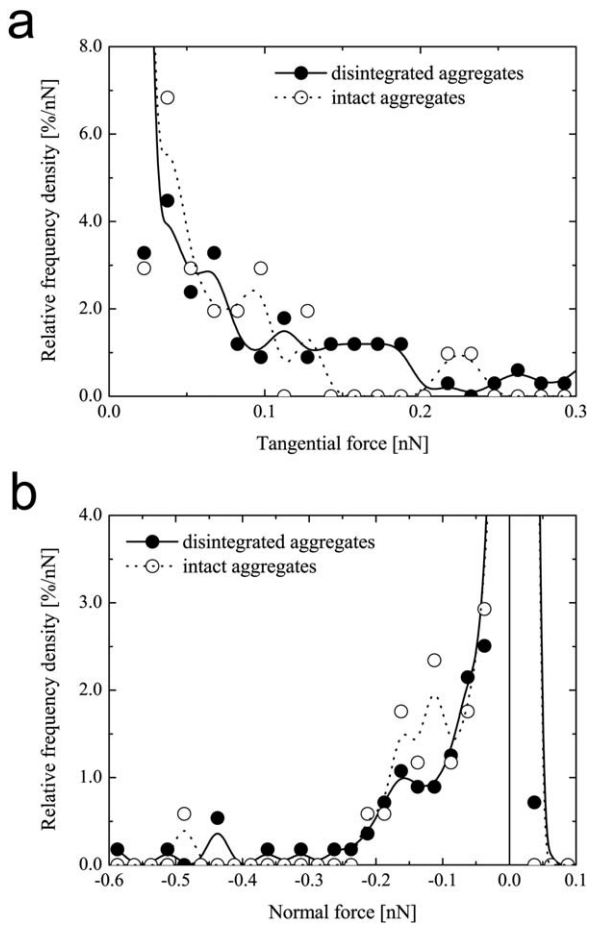

Figure 10. Density distribution of the bead contact force acting on aggregates under the conditions of Run 1: (a) tangential and (b) normal components.

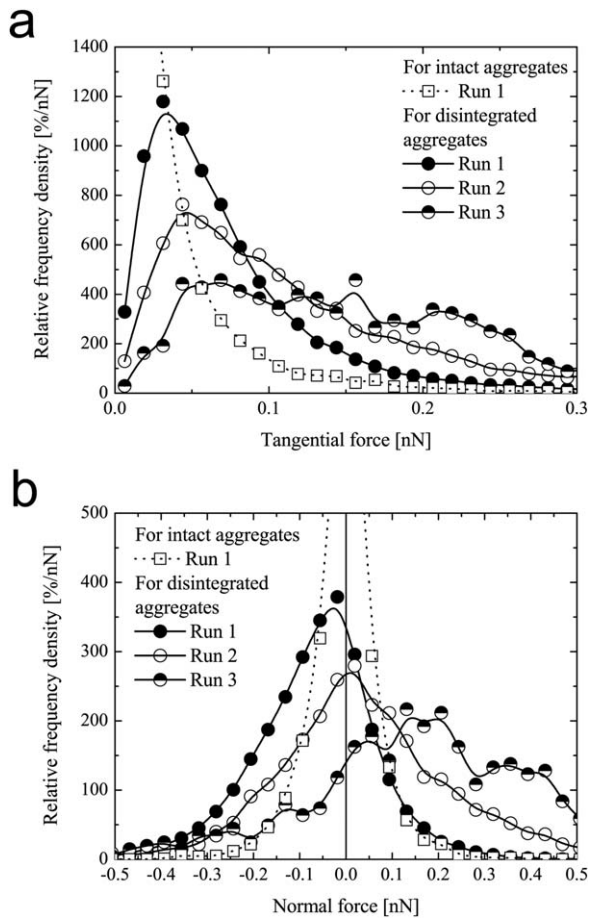

Figure 11. Density distribution of the fluid force acting on the aggregates: (a) tangential and (b) normal components.

According to this mechanism, the disintegration of strongly bonded aggregates by the bead contact force is difficult because the contact force only has the capability to compress aggregates, as shown in Figure 10b. In addition, under such conditions, there are few contact forces stronger than 0.1 nN (tangential) and −0.2 nN (normal), and this is similar to the tendency of the distribution for the fluid force acting on intact aggregates (Figure 11). Moreover, in Figure 10, it should be noted that even if the data used in the contact force distribution is that of disintegrated aggregates, the data is influenced by not only the contact force but also the fluid force because both these forces act on the aggregates at the same time. Thus, there is a high possibility that aggregates are disintegrated by the strong fluid force around the bead surface when aggregates are close to the beads and contact occurs. Therefore, the role of the beads is to induce the strong fluid force that disintegrates stronger aggregates. This confirms that the effective force for aggregate disintegration is the fluid force and not the contact force.

For the optimum design of the practical disintegration process of nanoparticles using a stirred media mill, the clarified disintegration mechanism indicates the importance of producing a bead motion and fluid flow in the mill that increases the fluid force, rather than the bead contact force, although the control of the bead contact force is significant for a comminution process design.[34] In practice, the bead size, stirring rate, and geometry of the mill significantly influence the bead motion and fluid flow. However, the precise nature of the effects of these parameters on the force applied to aggregates is unclear. Within these parameters, the stirring rate in the mill can be associated with the shear rate used in this simulation, and thus, the simulation can be used to investigate the effects of stirring rate and bead size on the force applied to aggregates, which will help us obtain a clear and more detailed mechanism of the disintegration process in a future study. Conversely, the effect of the mill geometry cannot be considered using a simple shear simulation; the coupled DEM–LES simulation used in our past study[14,15] that takes the mill geometry into account appeared to be an effective tool for designing the mill geometry in such a manner that the bead motion and fluid flow in the mill become desirable.

Conclusions

We have developed a numerical method for simulating the motion of beads and particulates (with a size ratio of 1000:1) coupled with fluid flow in a simple shear box. We were able to clarify the aggregate disintegration mechanism by using this simulation method to investigate different conditions and aggregation forces.

The simulation results confirmed that aggregates rarely collide with beads and revealed that the number ratio of disintegrated aggregates in collisions with beads was lower than 4%. In addition, the magnitude of the bead contact force acting on aggregates was too small to disintegrate aggregates under our simulation conditions. However, aggregates were effectively disintegrated by the effect of fluid flow with a high pure-shear rate around the bead surfaces. Aggregates with a strong aggregation force were disintegrated by the strong fluid force induced near the bead surface and also dominantly disintegrated by the expansive fluid force rather than the compressive fluid force. As a result, it was found that the effective force for the aggregate disintegration is the fluid force and not the contact force. Therefore, for the efficient disintegration of strong aggregates, it is important to develop regions with a strong fluid force by the efficient utilization of bead surfaces.

We hope that this information regarding the aggregate disintegration mechanism in a simple shear system will be useful for optimizing the design of the wet dispersion process using a stirred media mill. We are also interested in the influence of other parameters such as the bead diameter, shear rate, and slurry viscosity and how these relate to the bead contact force and fluid force in affecting aggregate disintegration; this will be the topic of future work.

Acknowledgment

This research was partially supported by JSPS KAKENHI Grant No. 23740304 (Grant-in-Aid for Young Scientists (B) to D. N.).

Literature Cited

1. Inkyo M, Tahara T. Dispersion of agglomerated nanoparticles by micromedia mill, ultra apex mill. *J Soc Powder Technol Jpn.* 2004; 41:578–589.
2. Inkyo M, Tahara T, Iwaki T, Iskandar F, Hogan CJ Jr, Okuyama K. Experimental investigation of nanoparticle dispersion by beads milling with centrifugal bead separation. *J Colloid Interface Sci.* 2006; 304(2):535–540.
3. Harigai K, Hashimoto K. Non-over loading dispersion technique using beads milling method. *J Jpn Soc Colour Mater.* 2006;79(4): 136–139.

4. Özcan-Taşk GN, Gavi E, Kubicki D, Wang Y. Dispersion of nanoscale silica particles using a novel design stirred bead mill. In: *Proceedings of 14th European Conference on Mixing*, Warsaw, Poland. September:353–358, 2012.
5. Cundall PA, Strack ODL. A discrete numerical model for granular assemblies. *Geotechnique*. 1979;29(1):47–65.
6. Cleary PW. DEM prediction of industrial and geophysical particle flows. *Particuology*. 2010;8(2):106–118.
7. Gudin D, Turczyn R, Mio H, Kano J, Saito F. Simulation of the movement of beads by the DEM with respect to the wet grinding process. *AIChE J*. 2006;52(10):3421–3426.
8. Yang RY, Jayasundara CT, Yu AB, Curry D. DEM simulation of the flow of grinding media in IsaMill. *Miner Eng*. 2006;19(10):984–994.
9. Eskin D, Zhupanska O, Hamey R, Moudgil B, Scarlett B. Microhydrodynamics of stirred media milling. *Powder Technol*. 2005;156(2):95–102.
10. Gers R, Climent E, Legendre D, Anne-Archard D, Frances C. Numerical modelling of grinding in a stirred media mill: hydrodynamics and collision characteristics. *Chem Eng Sci*. 2010;65(6):2052–2064.
11. Blecher L, Kwade A, Schwedes J. Motion and stress intensity of grinding beads in a stirred media mill. Part 1: energy density distribution and motion of single grinding beads. *Powder Technol*. 1996;86(1):59–68.
12. Theuerkauf J, Schwedes J. Theoretical and experimental investigation on particle and fluid motion in stirred media mills. *Powder Technol*. 1999;105(1):406–412.
13. Schilde C, Beinert S, Kwade A. Comparison of the micromechanical aggregate properties of nanostructured aggregates with the stress conditions during stirred media milling. *Chem Eng Sci*. 2011;66(21):4943–4952.
14. Nishiura D, Wakita Y, Shimosaka A, Shirakawa Y, Hidaka J. Estimation of power during dispersion in stirred media mill by DEM–LES simulation. *J Chem Eng Jpn*. 2010;43(10):841–849.
15. Shimosaka A, Asahi R, Nishiura D, Shirakawa Y, Hidaka J. Design of nanoparticle dispersion process in stirred media mill using DEM–LES coupling method. *J Chem Eng Jpn*. 2012;45(10):801–810.
16. Higashitani K, Iimura K. Two-dimensional simulation of the breakup process of aggregates in shear and elongational flows. *J Colloid Interface Sci*. 1998;204(2):320–327.
17. Higashitani K, Iimura K, Sanda H. Simulation of deformation and breakup of large aggregates in flows of viscous fluids. *Chem Eng Sci*. 2001;56(9):2927–2938.
18. Harada S, Tanaka R, Nogami H, Sawada M. Dependence of fragmentation behavior of colloidal aggregates on their fractal structure. *J Colloid Interface Sci*. 2006;301(1):123–129.
19. Nishiyama T, Inamuro T, Yasuda S. Numerical simulation of the dispersion of aggregated Brownian particles under shear flows. *Comput Fluids*. 2013;86:395–404.
20. Kajishima T, Takiguchi S, Hamasaki H, Miyake Y. Turbulence structure of particle-laden flow in a vertical plane channel due to vortex shedding. *JSME Int J Ser B*. 2001;44(4):526–535.
21. Tsuji Y, Kawaguchi T, Tanaka T. Discrete particle simulation of two-dimensional fluidized bed. *Powder Technol*. 1993;77(1):79–87.
22. Tsuji Y. Multi-scale modeling of dense phase gas–particle flow. *Chem Eng Sci*. 2007;62(13):3410–3418.
23. Briggs WL, McCormick SF, Henson VE. *A Multigrid Tutorial*, 2nd ed. Philadelphia: SIAM. 2000.
24. Nishiura D, Sakaguchi H. Parallel-vector algorithms for particle simulations on shared-memory multiprocessors. *J Comput Phys*. 2011;230(5):1923–1938.
25. Aoyama Y, Nakano J. *Rs/6000 sp: Practical MPI Programming*. New York: IBM. 1999.
26. Hertz H. On the contact of elastic solids. *J Reine Angew Math*. 1881;92:156–171.
27. Mindlin RD. Compliance of elastic bodies in contact. *J Appl Mech*. 1949;16:259–268.
28. Israelachvili JN. *Intermolecular and Surface Forces*, 3rd ed. London: Academic press. 2011.
29. Tsuji Y, Tanaka T, Ishida T. Lagrangian numerical simulation of plug flow of cohesionless particles in a horizontal pipe. *Powder Technol*. 1992;71(3):239–250.
30. Ergun S. Fluid flow through packed columns. *Chem Eng Prog*. 1952;48(2):89–94.
31. Wen CY, Yu YH. A generalized method for predicting the minimum fluidization velocity. *AIChE J*. 1966;12(3):610–612.
32. Simeonov JA, Calantoni J. Modeling mechanical contact and lubrication in Direct Numerical Simulations of colliding particles. *Int J Multiphase Flow*. 2012;46:38–53.
33. Zhang W, Noda R, Horio M. Evaluation of lubrication force on colliding particles for DEM simulation of fluidized beds. *Powder Technol*. 2005;158(1):92–101.
34. Jayasundara C, Yang R, Yu A. Discrete particle simulation of particle flow in a stirred mill: effect of mill properties and geometry. *Ind Eng Chem Res*. 2011;51(2):1050–1061.

Manuscript received May 6, 2014, and revision received Aug. 5, 2014.